International Journal of MATERIALS RESEARCH

Zeitschrift für METALLKUNDE

2007

Run-on print

Editor:
Deutsche Gesellschaft
für Materialkunde

Managing Editors:
M. Rühle
G. Petzow
P. P. Schepp

Carl Hanser Verlag
München

Volume 98

www.ijmr.de

HANSER

Robert F. Cook[a], Michelle L. Oyen[b]
[a]National Institute of Standards and Technology, Gaithersburg, USA
[b]Cambridge University Engineering Department, Cambridge, UK

Nanoindentation behavior and mechanical properties measurement of polymeric materials

During sharp contacts, polymeric materials can exhibit elastic (reversible), plastic (instantaneous irreversible), and viscous (time-dependent irreversible) deformation. Due to viscous effects commonly observed in experiments conducted on polymeric materials, the analytical methods developed for instrumented indentation testing ("nanoindentation") of elastic-plastic materials cannot be used to determine polymer mechanical properties. Here, a viscous-elastic-plastic sharp indentation model is reframed into normalized coordinates. The updated scheme allows the mechanical properties of polymeric materials to be determined simply from single- or multiple-cycle nanoindentation tests; output parameters are the relative resistance to plastic vs elastic deformation during indentation and the relative time scales for viscous flow during the contact event. The scheme allows the indentation behavior of all materials to be placed on a single map.

Keywords: Indentation; Nanoindentation; Viscoelastic; Viscous; Polymer

1. Introduction

Instrumented indentation testing (IIT), in which the load and displacement of a stiff, hard probe are monitored throughout a contact cycle on a material surface, has many advantages in determining the mechanical properties of materials. In conventional indentation testing, only the displacement at peak load is measured (e.g., Rockwell and Durometer tests) or inferred (from measurements of the residual contact impression, e.g., Brinell, Vickers, or Knoop tests) allowing a single material property – a characteristic contact stress, the "hardness" – to be determined [1, 2]. In most tests (Rockwell, Brinell, Vickers, Knoop) the hardness is related to, or taken as a direct measure of, the resistance to plastic deformation of the material, with acknowledgement in some cases (Rockwell, Vickers, Knoop) that there is also elastic deformation during the contact [3]. In the case where the hardness is a measure of the resistance of the material to elastic deformation (Durometer) there is acknowledgement that there could also be time-dependent deformation during the contact [2]. In common with conventional indentation tests, IIT requires only small samples with appropriately-prepared surfaces and provides a local measurement of material properties. Critical advantages of IIT over conventional indentation hardness tests, however, are that direct observation of the contact is not required (such that sub-microscopic measurements can be made, hence "nanoindentation") and IIT extends indentation testing to obtain both plastic and elastic properties of a material in the same test. An analysis of the unloading trace in IIT [4] allows the hardness (taken as the mean supported contact stress) and the plane-strain elastic modulus of a material to be determined, within the assumption that the material is elastically isotropic and that elastic deformation is the only deformation mode during unloading. A problem with extending IIT to materials with time-dependent mechanical properties (e.g., polymers, biological, and biomedical materials) is that the conventional analysis assumes no time dependence for the inelastic component of the contact deformation and is thus unable to assess unambiguously the elastic and plastic properties of a material. Conventional IIT also has no provision for measuring time-dependent mechanical properties, such as the viscosity.

The conveniences of IIT can be extended to assess the mechanical properties of polymeric materials in a non-quantitative way: Figure 1 shows characteristic load–displacement IIT "fingerprints" for some engineering materials, measured using a three-sided diamond pyramid Berkovich indenter. The almost completely closed hysteresis loop of the polyurethane, Fig. 1a, indicates a predominantly

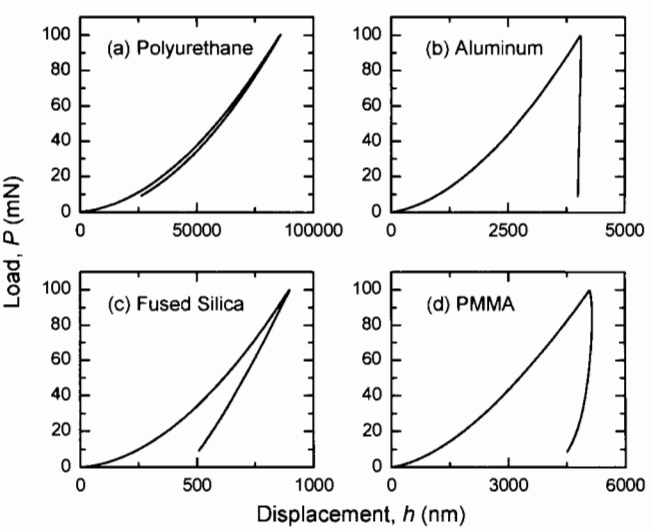

Fig. 1. Instrumented indentation load (P)-displacement (h) traces for four materials, displaying characteristic indentation behavior during Berkovich indentation: (a) Polyurethane, a predominantly elastic response; (b) Aluminum, a predominantly plastic response; (c) Fused silica, an elastic-plastic response; and (d) polymethylmethacrylate (PMMA), a viscous-elastic-plastic response. Triangle-wave loading, using a rise time of 100 s for all indentations.

elastic response (and thus explains the effectiveness of Durometer hardness tests used to measure the elastic properties of rubbery materials). The almost completely open hysteresis loop of the aluminum, Fig. 1b, indicates a predominantly plastic response (and thus explains the effectiveness of Vickers and Knoop hardness tests in measuring the plastic properties of metallic materials). The hysteresis loop of the fused silica, Fig. 1c, is only partially open and there is considerable elastic recovery on unloading, indicating a mixed elastic-plastic response (and it is exactly this sort of behavior exhibited by metals [4], ceramics [5], minerals [6], glasses [4, 7], and dielectrics [8, 9] that conventional IIT analysis describes so well). The hysteresis loop of the polymethylmethacrylate (PMMA), Fig. 1d, exhibits the open hysteresis loop characteristic of a plastic response and the recovery in the latter stages of unloading of an elastic response. In addition, it exhibits an increasing displacement during the initial stages of unloading and the characteristic forward-displacing "nose" [10], indicative of a viscous response, such that the overall behavior is viscous-elastic-plastic (VEP) [11]. Qualitative inspection of the IIT trace for a material and matching to IIT fingerprints such as in Fig. 1 allow the predominant or mixed deformation modes to be assessed.

Quantitative analysis of IIT traces has been studied extensively for elastic materials [12, 13], elastic-plastic materials (in which attention is focused on unloading) [4, 14], and viscoelastic materials (in which attention is focused on loading) [15, 16]. Here we describe a model developed [11] and used [17–19] previously for VEP materials based on a non-linear analogy with the time-dependent Maxwell deformation model often used for viscoelastic materials [20]. The VEP indentation model is re-formulated here to emphasize the material, indenter, and test parameters that separately influence the form of indentation load–displacement behavior. Emphasis is placed on the common indentation test protocol of load-controlled triangle wave loading with a hard, stiff pyramidal indenter and extended to cyclic loading. The ability of the model to describe the complete range of material indentation behavior, including that of polymeric materials as shown in Fig. 1, is demonstrated. An advantage of the reformulation is that it allows a mapping scheme to be developed (using dimensionless material, indenter, and test parameters) that enables indentation behavior of materials exhibiting a range of deformation modes to be represented on a single map.

2. Experimental observations

Time-dependent effects in the load-controlled indentation responses of polymeric materials are observed in three main ways. First, and most closely related to the conventional indentation test, is the observation that increasing the "rise time" (the time required to reach peak load) during triangle-wave loading leads to an increase in the observed residual contact impression dimensions, and thus decreased hardness. Increasing the rise time from 5 s to 500 s caused a doubling of the residual impression area on Berkovich indentation in PMMA [21]. Second, indentation creep is observed during "ramp and hold" loading, as shown in Fig. 2 for PMMA and polyurethane ramp loaded with a 20 s rise time and held at peak load for 120 s,

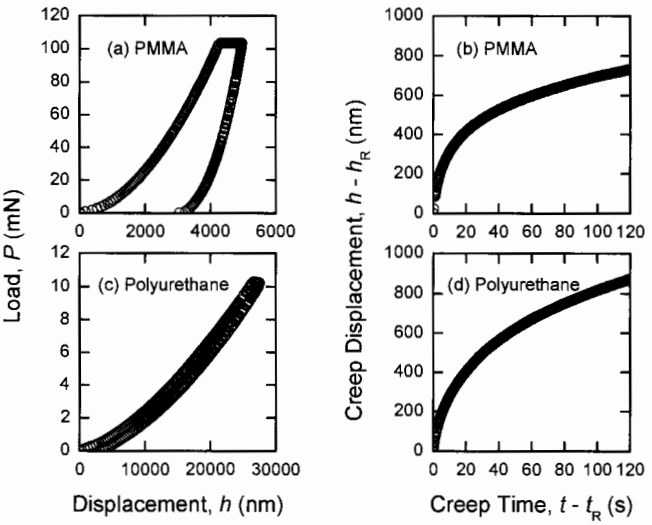

Fig. 2. Indentation behavior of PMMA and polyurethane, displaying the fixed-load creep responses following a 20 s ramp to peak load using a Berkovich indenter: (a, c) The indentation load (P)-displacement (h) traces for PMMA and polyurethane, respectively; (b, d) The creep displacement as a function of creep time, for PMMA and polyurethane, respectively.

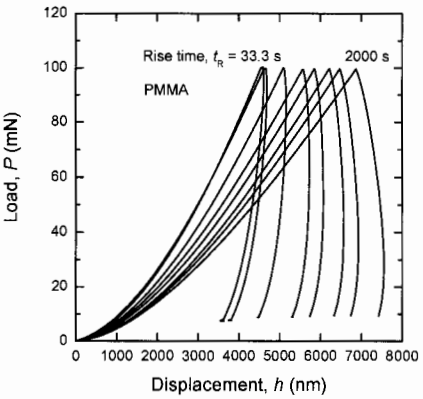

Fig. 3. Instrumented indentation load (P)-displacement (h) traces for PMMA, displaying increasing displacement with increasing rise time, for triangle-wave loading over the rise-time range indicated.

Fig. 2a and c. Significant fixed-load viscous creep is observed for both materials, although it is a much more substantial fraction of the contact deformation for PMMA, Fig. 2b, than polyurethane, Fig. 2d. Third, the shapes of load–displacement traces are observed to vary with rise time during triangle-wave loading to fixed peak load, as shown in Fig. 3 for PMMA with rise times varying from 33.3 s to 2000 s. For the shortest rise times, the material exhibited an almost elastic-plastic indentation fingerprint (cf. Fig. 1c). As the rise time was increased an indentation "nose" developed on unloading and the material exhibited the characteristic VEP indentation fingerprint (cf. Fig. 1d). For the longest rise times, there was almost no elastic recovery on unloading and the material exhibited a predominantly visco-plastic response. Clearly, as the rise time increased, there was much greater transient viscous creep, leading to a change in shape of the indentation response. It is the focus of the following analysis to describe the changes in shape observed in Fig. 3 in terms of material properties and test characteristics.

3. Analysis

The VEP indentation model considered here is formed from three quadratic deformation elements connected in pseudo-Maxwell series [11], as represented in Fig. 4. The plastic element, which is most simply related to the traditional hardness test, has a load–displacement relation on loading given by

$$P_P = \alpha_1 H h_P^2 \tag{1}$$

where P_P is the load, h_P is the plastic displacement, H is the plastic resistance, and α_1 is an indenter geometry constant given by $\alpha_1 = \pi \tan^2 \psi$ for an assumed rigid conical indenter of effective included angle 2ψ. The displacement remains at its peak-load value during unloading. For this element, the mean supported contact stress under load is the plastic resistance, H, often referred to in this context as the "true" hardness as it is associated only with plastic deformation and thus the yield resistance of the material [22]. Indentation of materials that behave approximately as rigid-perfectly plastic (such that the indentation deformation is predominantly plastic) can thus be used to measure the hardness and yield resistance from the remnant contact deformation, and in particular the surface contact dimension, $2a = 2h_P \tan \psi$ [1].

The elastic element has a reversible load–displacement relation given by

$$P_E = \alpha_2 M h_E^2 \tag{2}$$

where P_E is the load, h_E is the elastic displacement, M is the indentation modulus [23], and α_2 is an indenter geometry constant given by $\alpha_2 = \pi \tan \psi / 2\beta$ [13]. For a rigid conical indenter and an isotropic elastic material, the indentation modulus is the plane-strain modulus, E^*, of the material such that the contact stiffness $S = dP/dh = 2aE^*$, where the contact diameter is given by $2a = 2h_E \tan \psi/\beta$. Indentation of materials that behave approximately as elastic-perfectly plastic (such that the indentation deformation on unloading is predominantly elastic) can thus be used to measure the indentation or plane-strain modulus from the unloading stiffness. (Modifications of contact mechanics models accounting for the plastic deformation allow a to be estimated from S and the load and displacement at the onset of unloading [4].) The parameter $\beta - 1$ is the proportion of elastic deformation external to the contact relative to that internal to the contact [13, 24]: Consistent with the series model in which all deformation occurs within the contact [11], $\beta = 1$ is taken here.

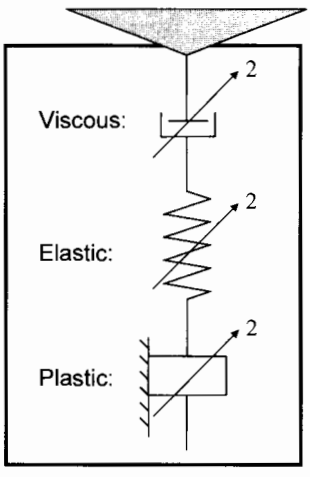

Fig. 4. Schematic diagram of the series viscous-elastic-plastic quadratic indentation model used in the current work. The total deformation due to indentation load is the sum of the deformations in each component.

The viscous element has an explicitly time-dependent load–displacement relation given by

$$P_V = \alpha_2 M \tau^2 (dh_V/dt)^2 \tag{3}$$

where P_V is the load, h_V is the viscous displacement, and τ is the time constant for viscous flow. As in analyses of *viscoelastic* deformation and indentation, the form of the constitutive law for the time-dependent deformation must be selected with a view to describing the empirical observations [20]. For example, in many cases the combination of two linear elastic elements and a linear viscous element to form a standard linear solid (SLS) is taken for modeling homogeneous linearly viscoelastic responses [20]. For the indentation case considered here, a quadratic viscous element is taken, for which the underlying non-linear viscous flow law is $\sigma \propto \dot{\varepsilon}^2$, where σ is a characteristic indentation stress and ε is a characteristic indentation strain rate (the combination $\alpha_2 M \tau^2$ is then an effective quadratic viscosity). The term viscous is taken here as a simple reference to time-dependent deformation without regard to deformation mechanism: poroelastic deformation, or other behavior more generally referred to as "creep", could also be described in this way.

As the deformation elements are taken in series, the total displacement, h, is the sum of the individual displacement elements,

$$h = h_V + h_E + h_P \tag{4}$$

and the load, P, is common to all elements,

$$P = P_V = P_E = P_P \tag{5}$$

The indentation protocol considered here is load control using a triangle-wave load function. On loading,

$$P = P_{max}(t/t_R), \quad 0 \le t \le t_R \tag{6}$$

where t is the time, and t_R is the rise time required to reach maximum or peak load, P_{max}. On unloading,

$$P = P_{max}(2 - t/t_R), \quad t_R \le t \le 2t_R \tag{7}$$

Direct substitution and simple integration of the time-dependence of the load gives the displacements during loading as (combining Eqs. (1)–(3) and (6))

$$h_P = \left(\frac{P_{max} t}{\alpha_1 H t_R}\right)^{1/2}, \quad h_E = \left(\frac{P_{max} t}{\alpha_2 M t_R}\right)^{1/2}$$
$$h_V = \frac{2}{3}\left(\frac{P_{max} t^3}{\alpha_2 M \tau^2 t_R}\right)^{1/2} \tag{8}$$

with corresponding values at the rise time (peak load) of

$$h_{PR} = \left(\frac{P_{max}}{\alpha_1 H}\right)^{1/2}, \quad h_{ER} = \left(\frac{P_{max}}{\alpha_2 M}\right)^{1/2}$$
$$h_{VR} = \frac{2t_R}{3\tau}\left(\frac{P_{max}}{\alpha_2 M}\right)^{1/2} \tag{9}$$

During loading there is no distinction between the functional form of the elastic and plastic components and only the viscous component of the displacement at peak load has an explicit dependence on the rise time. At peak load, the three displacement components, Eq. (9), are related by two dimensionless ratios:

$$h_{PR} = \left(\frac{\alpha_2 M}{\alpha_1 H}\right)^{1/2} h_{ER}, \quad h_{VR} = \frac{2t_R}{3\tau} h_{ER} \tag{10}$$

such that the total displacement at peak load, h_R, is given by

$$h_R = h_{PR} + h_{ER} + h_{VR} = h_{ER}\left[1 + \left(\frac{\alpha_2 M}{\alpha_1 H}\right)^{1/2} + \frac{2t_R}{3\tau}\right] \tag{11}$$

On unloading, the three displacement components exhibit distinctive behavior: The plastic displacement remains fixed at the peak-load value, the elastic displacement recovers, and the viscous component continues to increase, (combining Eqs. (1)–(3) and (7)) according to

$$h_P = h_{PR}, \quad h_E = \left[\frac{P_{max}(2 - t/t_R)}{\alpha_2 M}\right]^{1/2}$$
$$h_V = \frac{2t_R}{3\tau}\left(\frac{P_{max}}{\alpha_2 M}\right)^{1/2}\left[2 - (2 - t/t_R)^{3/2}\right] \tag{12}$$

with corresponding final values at the end of the contact cycle of

$$h_{PF} = h_{PR}, \quad h_{EF} = 0, \quad h_{VF} = 2h_{VR} \tag{13}$$

In order to explore the range of VEP indentation responses it is convenient to introduce normalizations for the experimental measurables of displacement, time, and load of

$$\tilde{h} = \frac{h}{h_R}, \quad \tilde{t} = \frac{t}{t_R}, \quad \tilde{P} = \frac{P}{P_{max}} \tag{14}$$

Parameters describing the normalized material behavior include the dimensionless ratios introduced earlier (Eq. 10),

$$y = \left(\frac{\alpha_1 H}{\alpha_2 M}\right)^{1/2}, \quad d = \frac{3\tau}{2t_R}, \quad \frac{1}{e} = 1 + \frac{1}{y} + \frac{1}{d} \tag{15}$$

and these parameters have simple physical interpretations: y is a measure of a characteristic indentation yield strain (a stress divided by a modulus) [1], d is related to the Deborah number for the contact event (a material time constant divided by a test or observation time) [25], and e is the proportion of elastic deformation at peak load (the proportions of plastic and viscous deformation at peak load are e/y and e/d, respectively). With these normalizations, the loading and unloading cycles are represented simply as

$0 \le \tilde{t} \le 1$ (loading, Eq. (8))

$$\tilde{P} = \tilde{t}, \quad \tilde{h}_P = (e/y)\,\tilde{t}^{1/2}, \quad \tilde{h}_E = e\tilde{t}^{1/2}, \quad \tilde{h}_V = (e/d)\tilde{t}^{3/2} \tag{16}$$

and $1 \le \tilde{t} \le 2$ (unloading, Eq. (12))

$$\tilde{P} = (2 - \tilde{t}), \quad \tilde{h}_P = (e/y), \quad \tilde{h}_E = e(2 - \tilde{t})^{1/2}$$
$$\tilde{h}_V = (e/d)\,[2 - (2 - \tilde{t})^{3/2}] \tag{17}$$

In both cases, the total normalized displacement, $\tilde{h}$, is given by, Eq. (4),

$$\tilde{h} = \tilde{h}_P + \tilde{h}_E + \tilde{h}_V \tag{18}$$

such that $\{\tilde{P}, \tilde{t}\}$ and $\{\tilde{h}, \tilde{t}\}$ form a parametric set for $\{\tilde{P}, \tilde{h}\}$. With these normalizations, the $\{\tilde{h}, \tilde{t}\}$ loading and unloading trajectories end and begin, respectively, at $\{1, 1\}$. Note that in these *normalized* coordinates, the form for both loading and unloading is entirely defined by *two* parameters from e, y, and d, as the scale is fixed. In absolute coordinates three parameters are required to describe the behavior.

Figure 5a shows an example of an $\{\tilde{h}, \tilde{t}\}$ displacement trajectory and its components, for typical VEP indentation parameters of $y = 0.5$, $d = 1.5$. During loading, the plastic and elastic components increase in a concave manner to their maximum, peak-load values at the rise time, at which point there is a discontinuity in the derivative of their displacement-time trajectories associated with the discontinuity in the imposed load-time trajectory. On unloading, the plastic component remains fixed and the elastic component recovers to zero. On loading, the viscous component also increases, but in a convex rather than concave manner reflecting the increasing displacement rate with increasing load. At peak load and unload there is no discontinuity in the viscous displacement-time derivative as there is no discontinuity in load. On unloading, the viscous component

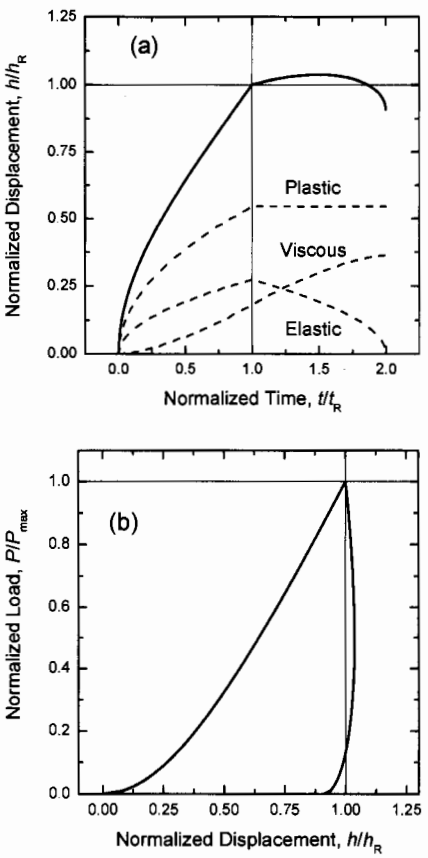

Fig. 5. (a) Normalized displacement–normalized time ($\tilde{h} = h/h_R$, $\tilde{t} = t/t_R$) responses for the component (viscous, elastic and plastic) deformations ($\tilde{h}_V, \tilde{h}_E, \tilde{h}_P$) and the total deformation ($\tilde{h}$). (b) Normalized load–normalized displacement ($\tilde{P} = P/P_{max}$, $\tilde{h} = h/h_R$) response for the normalized displacement–time data shown in part (a) with triangle-wave ramp loading at fixed loading- and unloading-rates, P_{max}/t_R.

increases in a concave manner. The complete trajectory increases in a weakly concave manner during loading, as the forms of the viscous, elastic, and plastic components compete. There is a discontinuity in the total displacement derivative at the rise time and continued increase in the displacement after the rise time, reflecting the dominance of the viscous component in the middle of the contact cycle. Finally, there is a strongly concave response and recovery to a non-zero final displacement, reflecting the dominance of the elastic and plastic components towards the end of the cycle. Figure 5b shows the related $\{\tilde{P}, \tilde{h}\}$ load–displacement trace. Over the full contact cycle it exhibits hysteresis indicative of the plastic and viscous deformation components. In the unloading cycle, it exhibits the characteristic forward-displacing "nose" indicative of a significant viscous deformation component. The similarity of the trace to the experimental observations of PMMA in Figs. 1 and 3 is obvious.

Displacement-time trajectories and related load–displacement traces for cyclic loading are easily extended from the single-cycle equations given above. For the ith load-unload cycle these are (loading)

$$\tilde{P} = \tilde{t} - 2(i-1), \quad \tilde{h}_P = (e/y)\left[\delta_{1i}\tilde{t}^{1/2} + (1-\delta_{1i})\right]$$

$$\tilde{h}_E = e[\tilde{t} - 2(i-1)]^{1/2} \tag{19}$$

$$\tilde{h}_V = (e/d)\left[2(i-1) + [\tilde{t} - 2(i-1)]^{3/2}\right]$$

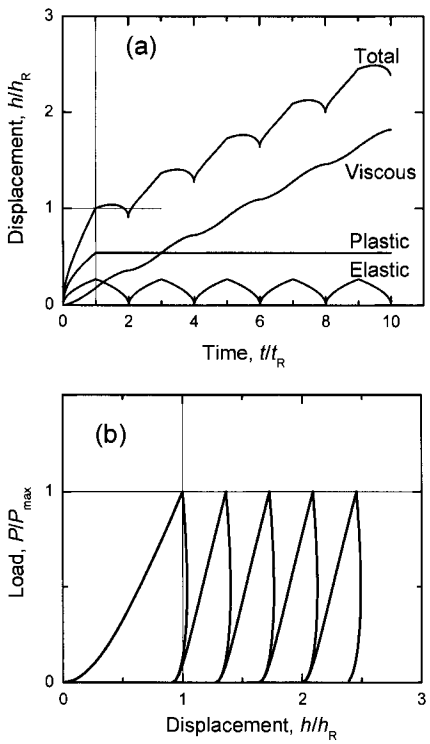

Fig. 6. (a) Normalized displacement–normalized time ($\tilde{h} = h/h_R$, $\tilde{t} = t/t_R$) responses for the component (viscous, elastic and plastic) deformations ($\tilde{h}_V, \tilde{h}_E, \tilde{h}_P$) and the total deformation ($\tilde{h}$) in a cyclic test with five individual loading- and unloading-cycles. (b) Normalized load–normalized displacement ($\tilde{P} = P/P_{max}$, $\tilde{h} = h/h_R$) response for the normalized displacement–time data shown in part (a) with triangle-wave ramp loading at fixed loading- and unloading rates P_{max}/t_R for five cycles.

and (unloading)

$$\tilde{P} = 2i - \tilde{t}, \quad \tilde{h}_P = (e/y), \quad \tilde{h}_E = e(2i-\tilde{t})^{1/2}$$
$$\tilde{h}_V = (e/d)\left[2i - (2i-\tilde{t})^{3/2}\right] \tag{20}$$

where δ_{1i} is the Krönecker delta. Figure 6a and b show the calculated $\{\tilde{h}, \tilde{t}\}$ and $\{\tilde{P}, \tilde{h}\}$ behavior for five contact cycles using the same parameters as Fig. 5. There are two important features in Fig. 6: Figure 6a highlights the differences in the time-dependent behavior of the three deformation modes, but in particular illustrates that over time the total cumulative deformation is dominated by the viscous component. Figure 6b illustrates the so-called "first-cycle" effect: The plastic deformation component only changes during the first loading half-cycle, and hence all unloading half-cycles are identical, as are all load–displacement traces subsequent to the first, which has the largest degree of hysteresis. The following section will use the normalized forms for load and displacement, along with the dimensionless y and d parameters, to explore and map the range of VEP indentation behavior.

4. Indentation behavior maps

A measure of indentation behavior is the distribution of the three deformation modes within the total deformation at peak load in the first contact cycle. Such a measure will of course depend on the material, the indenter geometry, and the time-scale of the contact event. As noted above, the parameters e, e/y, and e/d are the proportions of elastic, plastic, and viscous deformation at peak load in the first cycle. Large values of y lead to small amounts of plastic deformation, and hence y characterizes the indentation plastic yield resistance (the physical meaning of large y is that the yield stress of the material is large–relative to the modulus–so that plastic deformation by indentation is difficult). Large values of d lead to small amounts of viscous deformation, and hence d characterizes the indentation viscous flow resistance (the physical meaning of large d is that the contact cycle is rapid–relative to the viscous deformation time scale–so that viscous flow during indentation is truncated).

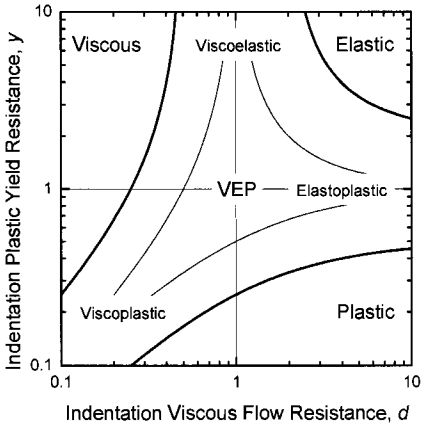

Fig. 7. Behavior map cross-plotting the two material descriptors: the relative plastic yield resistance (y) and the indentation viscous flow resistance (d). The bold contour lines indicate regions where the indentation deformation at peak load is 2/3 of the type labeled, and the central region ($y = d = 1$) represents fully-developed viscous-elastic-plastic behavior.

The parameters y and d are convenient co-ordinates to map regions of indentation behavior: fixing the proportion of a deformation mode allows a locus in (y, d) space to be calculated that describes a contour on the map, as shown in Fig. 7. The bold contour lines indicate regions where the indentation deformation at peak load is 2/3 of the type labeled. Regions inside these contours away from the center indicate indentation behavior dominated by one deformation mode. The fine contour lines indicate regions where the indentation deformation at peak load is 1/2 of the type labeled. Regions close to two fine contour lines away from the center indicate indentation behavior dominated by two deformation modes. The central region enclosed by the three fine contour lines indicates indentation behavior including all three deformation modes.

Characteristic indentation load–displacement responses occur for yield and flow resistance parameters located on various positions on the map are shown in Fig. 8, using Eqs. (19) and (20) to calculate three load-unload cycles in the normalized coordinates. The yield and flow resistance parameters used reflect the mid-range for the characteristic responses, as shown in Table 1. The elastic response (E), in the top-right corner, exhibits considerable displacement recovery (here about 65 %) on unloading from the peak load and little distinction between the first and subsequent cycles in the shape and size of the load–displacement hysteresis loops. This is the characteristic load–displacement response of rubbery, elastomeric, materials such as polyurethane. On decreasing the indentation yield resistance to generate an elastoplastic response (EP), the extent of unloading recovery decreases and hysteresis loops subsequent to the first are much smaller. This is the characteristic load–displacement response of hard metals, ceramics, minerals, silicate glasses, and hard dielectric films, and many indentation analyses have been directed at interpreting such responses. On decreasing the yield resistance even further to generate a predominantly plastic response (P), the "first cycle" effect is extreme and there are negligible hysteresis loops subsequent to the first cycle. This is the characteristic load–displacement response of soft metals [4], ceramic [26] and metal foams [27], and nanoporous low-dielectric-constant films [9]. The almost-linear unloading response, displaying little of the convexity of the loading response, or that of the more elastic systems, was the subject of early instrumented indentation analyses [28].

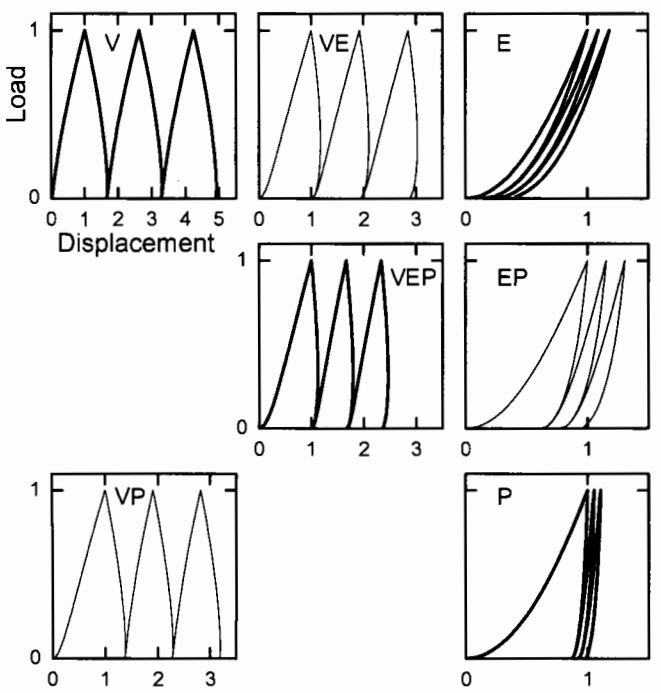

Fig. 8. Characteristic indentation (normalized) load–displacement (P/P_{max}, h/h_R) responses for dominantly viscous (V), elastic (E), plastic (P), viscoelastic (VE), viscoplastic (VP), elastoplastic (EP) and fully-developed viscous-elastic-plastic (VEP) behavior, arranged to correspond to the mechanism map shown in Fig. 7. The responses are computed for three triangle-wave load-unload cycles in the normalized coordinates using the parameters shown in Table 1.

Conversely, although the extent of recovery decreases, on decreasing the viscous flow resistance of the elastic system (E) to generate a viscoelastic response (VE), the hysteresis loops increase in size, with little first-cycle effect. In addition, the loading response becomes almost linear and the unloading response is initially mildly concave before becoming mildly convex. The unloading response can also be characterized by an initial positive unloading slope and unloading "nose", and these are the characteristics of the load–displacement responses of polymers, and silicate and chalcogenide glasses at elevated temperatures [29]. Such responses have been the subject of indentation analyses based loosely on elastic-viscoelastic correspondence principles [29]. On further decreasing the viscous flow resistance, a predominantly viscous response is generated (V) that is characterized by concave loading and unloading curves and little distinction between the hysteresis loops. (This would presumably be the indentation response of thermoplastic polymers and inorganic glasses at high temperatures.) Decreasing the plastic yield resistance from this point generates a viscoplastic response (VP) that exhibits a mild first-cycle effect and smaller, but still concave, subsequent hysteresis loops and no recovery. (This would presumably be the indentation response of metals at elevated

Table 1. Characteristic indentation deformation mode and deformation mode parameters.

Characteristic Deformation Mode	Deformation Mode Proportion	Indentation Yield Resistance, y	Indentation Flow Resistance, d
Viscous (V)	0.81	6	0.2
Elastic (E)	0.91	20	20
Plastic (P)	0.81	0.2	6
Viscoelastic (VE)	0.92	6	1
Elastoplastic (EP)	0.92	1	6
Viscoplastic (VP)	0.91	0.2	0.2
Viscous-Elastic-Plastic (VEP)	1	1	1

temperature with both fast and slow plastic deformation mechanisms and perhaps glassy, thermosetting, polymers.)

The central VEP response of Fig. 8 exhibits the characteristics of all three deformation modes: the recovery associated with reversible elastic deformation; the first-cycle effect associated with irreversible plastic deformation; and the nose associated with time-dependent viscous deformation. It is important to recognize that the coordinates used here to characterize indentation behavior include both material properties and indentation contact variables, and thus both can influence the balance between the deformation modes during a contact event. Materials with large hardness/modulus ratios (H/M) or large time constants (τ) for flow will obviously tend to viscoelastic or elastoplastic responses as plastic or viscous deformation, respectively, are suppressed. However, indentation contacts with probes of large acuity ($\cot\psi$) or that extend over a large period of time (t_R) counter these effects by imposing large amounts of shear (and thus driving plastic deformation) or long contact periods (and thus enabling viscous deformation; the driving force for viscous deformation may also be increased by large acuity probes). Hence large-acuity pyramidal probes (Vickers or cube-corner, [30]) loaded for relatively short contact times are used to study elastoplastic indentation in ceramics and dielectrics and small acuity spherical probes loaded for relatively long contact times are used to study viscoelastic indentation in polymers [31].

5. Discussion

The three distinctive displacement trajectories exhibited by the three deformation modes on unloading, Fig. 4, suggest the experimental, normalized $\{\tilde{h}, \tilde{t}\}$ trajectory is convenient for determining the material indentation properties τ, M, H. After extracting the unloading data and normalizing by the measured values of h_R and t_R, the data can be fit to Eqs. (17) and (18) to obtain y, d, and e, noting that only two of the three are independent. Usually the first two parameters will be best as fitting variables as they have most obvious physical meaning. For initial estimates of y, it is useful to know that the equivalent cone angle for Berkovich or Vickers indenters commonly used in instrumented indentation testing is $\psi = 70.3°$ and thus $(\alpha_1/\alpha_2)^{1/2} = (2\tan\psi)^{1/2} \approx 2.36$. The advantage of fitting in these normalized coordinates is that only shape matters and that all quantities are of order 0.1 to 10. Once the fitting parameters are found, the material properties can be obtained from the deconvolution relations

$$\tau = \frac{2t_R d}{e}$$

$$M = \frac{P_{max}}{\alpha_2 h_R^2 e^2} \tag{21}$$

$$H = \frac{P_{max} y^2}{\alpha_1 h_R^2 e^2}$$

It is then a simple matter to use these parameters to predict responses for other loading protocols using the master VEP constitutive equations, Eqs. (1)–(5), in the general case [11], or the triangle-wave solutions, Eqs. (6)–(9), as appropriate. Figure 9 shows an example of the latter. The solid lines are fits to the unloading data and predictions of the loading data for the extremes and a central rise time from the PMMA data in Fig. 3. The ability of the model to describe VEP indentation behavior over a factor of 60 in rise time and predict the complete indentation cycle is obvious.

The limitations of the model in its current form, however, are apparent in Table 2, which lists the parameters describing the fits in Fig. 9. The material properties, τ, M, H, all vary with rise time, indicative of a strong Deborah number effect. That is, the apparent time constant describing material flow behavior varied with the observation time of the test. This suggests that there were multiple flow mechanisms occurring within the material, each with a characteristic time scale, and that changing the rise time altered the relative magnitude of the contribution to the total displacement from an individual mechanism. Perhaps unsurprisingly, the apparent time constant increased with rise time, suggesting that as the observation time was increased the test sampled slower material flow processes characterized

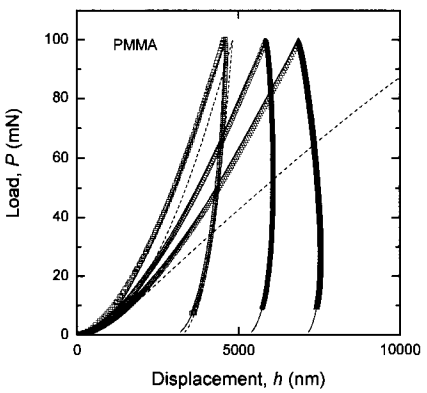

Fig. 9. Instrumented indentation load–displacement (P–h) traces for PMMA, displaying the central (t_R = 333 s) and extreme (t_R = 33.3 s and t_R = 2000 s) responses from Fig. 3 (open symbols). The solid lines are fits to each response using the VEP model, while the dashed lines are predictions for the 33.3 s and 2000 s data based on the fit at 333 s.

Table 2. Indentation deformation parameters for PMMA.

Rise Time, t_R (s)	Displacement at Rise Time, h_R (nm)	Plastic Yield Resistance, y	Viscous Flow Resistance, d	Elastic Fraction, e	Time Constant, τ (s)	Indentation Modulus, M (GPa)	Hardness, H (GPa)
33.3	4595	1.33 ± 0.04	3.55 ± 0.03	0.492 ± 0.019	78.9 ± 3.1	4.46 ± 0.34	1.41 ± 0.14
333	5860	0.608 ± 0.007	1.552 ± 0.002	0.304 ± 0.004	344 ± 5	7.18 ± 0.19	0.476 ± 0.17
2000	6869	0.373 ± 0.005	0.900 ± 0.003	0.209 ± 0.004	1200 ± 23	11.08 ± 0.42	0.276 ± 0.13

(Uncertainties represent single standard deviations.)

by longer time constants. The single time constant used in the VEP model averaged over all flow processes occurring in the material and thus increased with rise time. This limitation has also been observed in viscoelastic analyses of spherical IIT of polymers. The single time constant SLS model is inadequate to describe experimental observations and a two- or three- time constant extended SLS model is required [31, 32]. The inability of a single time constant model to describe the complete range of indentation behavior is indicated by the dashed lines in Fig. 9: these are predictions of the extreme responses from the parameters describing the central response. The short rise-time data are reasonably predicted, but the prediction for the long rise-time data grossly overestimates the displacement at a given load as the assumed time constant is too small and the model therefore overpredicts the transient viscous creep.

Multiple time constants in viscoelastic solid models are obtained by placing several Kelvin (parallel elastic-viscous) elements in series with an additional elastic element, or by placing several Maxwell (series elastic-viscous) elements in parallel to an additional elastic element [20, 33]. In both cases the limiting behavior is a fixed, equilibrium response. The construction of these solid models highlights a feature of the VEP model that may or may not be a limitation: The model is strictly a pseudo-Maxwell *fluid* model, as the viscous element is unconstrained by an elastic element in parallel. As observed in Fig. 5, continued loading leads to continued flow (there are no free viscous elements in the above-described solid models and flow is curtailed after a characteristic time). A natural extension of the VEP model is then to form a flow-constrained, multiple time-constant model by the addition of a flow-constraining elastic element and additional viscoelastic terms (Kelvin or Maxwell elements). Whether the indentation behavior of a material is more solid-like (described by an unconstrained elastic element) or fluid-like (unconstrained viscous element), of course, will depend on Deborah number considerations. A simple experimental method to determine the best form for the viscous component of the displacement is analysis, over the time scale of interest, of fixed-load indentation creep, Fig. 2, as the elastic and plastic components are invariant during such a test.

The VEP model is formulated in the extensive coordinates of load, P, and displacement, h, of the indentation system. The differential constitutive equation relating these two for an arbitrary contact history is of the form [11]

$$\frac{dh}{dt} = AP^{1/2} + B\frac{dP^{1/2}}{dt} \tag{22}$$

where A and B are constants and which is homogeneous in $P^{1/2}$. This homogeneity leads to a similarity of the $\{P, h\}$ responses obtained for similar contact histories, i. e., the loads and displacements of the responses and histories are scaled by a common factor – the shape is invariant, providing the time scale of the contact event is invariant. This is what is observed experimentally [11] (at least for simple contact histories, such as the triangle-wave used here) and should provide a constraint on the form of multi-time-scale models.

Some approaches to modeling pyramidal indentation of *viscoelastic* materials [16, 34] using elastic-viscoelastic correspondence are based on linear viscoelastic elements and thus the governing differential equation is homogeneous in the stress and strain. This in turn leads to inhomogeneity in the differential equation for the load and displacement. In contrast, the VEP model here is based on a nonlinear viscoelastic constitutive law, and thus has a related stress–strain differential equation that is inhomogeneous. The differentials for the characteristic stress and strain are given by $d\sigma \propto dP/h^2$ and $d\varepsilon \propto dh/h$, respectively, such that using Eqs. (1)–(3) leads to

$$\frac{d\varepsilon}{dt} = A\sigma^{1/2} + B\frac{d\sigma}{dt} \tag{23}$$

where once again A and B are constants and which is inhomogeneous in σ. Interestingly, the linear viscoelastic approach has been demonstrated to be a poor descriptor of pyramidal indentation creep data [34] while the VEP nonlinear viscoelastic approach has demonstrated promise in describing observed experimental data [11, 17–19]. The apparent nonlinear viscoelasticity in pyramidal indentation may be due to the large strains imposed by the relatively acute indenter geometry [21].

6. Conclusions

The inclusion of time-dependent, viscous deformation, common in polymeric materials, leads to a wide variety of indentation load–displacement traces beyond the usual range of hysteresis loops observed for elastic-plastic materials during IIT. In particular, general VEP indentation behavior during triangle-wave loading may include a negative initial unloading tangent and a forward-displacing nose if the viscous and elastic deformation components are comparable, no recovery on unloading if the viscous deformation dominates the elastic deformation, or no first-cycle effect if the viscous deformation dominates the plastic deformation.

A three-element, non-linear, VEP model can be used to describe the full range of indentation behavior, including these time-dependent effects. The model is formulated in the indentation load and displacement coordinates and incorporates the physically-interpretable material parameters of a plastic yield resistance (related to the yield stress) and a viscous flow resistance (related to the Deborah number of the material/test time scale ratio).

These resistance parameters are convenient coordinates in the formation of an indentation behavior map, which allows the indentation responses of all materials to be placed on a single map and the effects of test time and indenter acuity to be incorporated.

Although the model is able to describe complete responses in quantitative detail for a given indentation, the single time constant in the current formulation limits the ability to extrapolate time constant, modulus, and hardness parameters over large time scales. However, provided indentation times are similar, the simple scheme developed for obtaining these material properties from load–displacement–time data make this approach extremely useful for material-material comparisons between specimens and for within-material comparisons on different locations on a sample.

References

[1] D. Tabor: The Hardness of Metals, Oxford University Press (at the Clarendon Press), London (1951).
[2] ASTM D2240-0, Standard Test Method for Rubber Property–Durometer Hardness (Types A, B, C, D, DO, E, M, O, OO, OOO, OOO-S, and R).
[3] B.R. Lawn, V.R. Howes: J. Mater. Sci. 16 (1981) 2745.
[4] W.C. Oliver, G.M. Pharr: J. Mater. Res. 7 (1992) 1564.
[5] J. Thurn, R.F. Cook: J. Mater. Res. 19 (2004) 124.
[6] M.E. Broz, R.F. Cook, D.L. Whitney: Am. Mineral. 91 (2006) 135.
[7] D.J. Morris, R.F. Cook: J. Am. Ceram. Soc. 87 (2004) 1494.
[8] R.F. Cook, E.G. Liniger: J. Electrochem. Soc. 146 (1999) 4439.
[9] Y. Toivola, J. Thurn, R.F. Cook: J. Electrochem. Soc. 149 (2002) F9.
[10] B.J. Briscoe, L. Fiori, E. Pelillo: J. Phys. D: Appl. Phys. 31 (1998) 2395.
[11] M.L. Oyen, R.F. Cook: J. Mater. Res. 18 (2003) 139.
[12] H. Hertz: Miscellaneous Papers (translated by Jones, D.E., Schott, G.A.), Macmillan and Co., London (1896), 178–180.
[13] I.N. Sneddon: Int. J. Engng. Sci. 3 (1965) 47.
[14] J.S. Field, M.V. Swain: J. Mater. Res. 8 (1993) 297.
[15] E.H. Lee, J.R.M. Radok: J. Appl. Mech. 27 (1960) 438.
[16] H. Lu, B. Wang, J. Ma, G. Huang, H. Viswanathan: Mech. Time-dep. Mater. 7 (2003) 189.
[17] M.L. Oyen, R.F. Cook, N.R. Moody, J.A. Emerson: J. Mater. Res. 19 (2004) 2487.
[18] F. Mammeri, E. Le Bourhis, L. Rozes, C. Sanchez, A. Huignard, D. Lefevre: J. Non-Crystall. Solids 345 & 346 (2004) 610.
[19] M.L. Oyen, C.-C. Ko: J. Mater. Sci. Mater. Med. (2006), in press.
[20] W.N. Findley, J. Lai, K. Onaran: Creep and Relaxation of Nonlinear Viscoelastic Materials, Dover, New York (1989).
[21] M.L. Oyen: Philos. Mag. 86 (2006) 5625.
[22] M. Sakai: J. Mater. Res. 14 (1999) 3630.
[23] J.J. Vlassak, W.D. Nix: Philos. Mag. A 67 (1993) 1045.
[24] A.E.H. Love: Treatise on the Mathematical Theory of Elasticity, 3rd Edition, Dover, New York (1944).
[25] C. Macosko: Rheology, Wiley-VCH, New York (1994).
[26] Y. Toivola, A. Stein, R.F. Cook: J. Mater. Res. 19 (2004) 260.
[27] M.F. Ashby, A.G. Evans, N.A. Fleck, L.J. Gibson, J.W. Hutchinson, H.N.G. Wadley: Metal Foams: A Design Guide, Butterworth-Heinemann (Elsevier), Burlington, MA (2000).
[28] M.F. Doerner, W.D. Nix: J. Mater. Res. 1 (1986) 601.
[29] M. Sakai, S. Shimizu: J. Non-Crystall. Solids 282 (2001) 236.
[30] D.J. Morris, S.B. Myers, R.F. Cook: J. Mater. Res. 19 (2004) 165.
[31] M.L. Oyen: J. Mater. Res. 20 (2005) 2094.
[32] J.M. Mattice, A.G. Lau, M.L. Oyen, R.W. Kent: J. Mater. Res. 21 (2006) 2003.
[33] G.T. Mase, G.E. Mase: Continuum Mechanics for Engineers, 2nd Ed., CRC, Boca Raton, FL (1999).
[34] C.A. Tweedie, K.J. Van Vliet: J. Mater. Res. 21 (2006) 1576.

(Received October 11, 2006; accepted January 14, 2007)

Correspondence address

Robert F. Cook
Ceramics Division
National Institute of Standards and Technology
100 Bureau Drive, Mail Stop 8520
Gaithersburg, MD 20899, USA
Tel.: +1 301 975 3207
Fax: +1 301 975 5334
E-mail: robert.cook@nist.gov